Predicting the Phase Diagram of a Liquid Crystal Using the Convex Peg Model and the Semiempirical PM3 Method

Eduardo García-Sánchez,[†] Antonio Martínez-Richa,*[,†] José Antonio Villegas-Gasca,[†] Luis Humberto Mendoza-Huizar,[†] and Alejandro Gil-Villegas[‡,§]

Facultad de Química, Universidad de Guanajuato, Noria Alta s/n, Guanajuato, Gto., 36050, México, Instituto de Física, Universidad de Guanajuato, Lomas del Bosque 103, León, Gto., 37150, México, and Molecular Engineering Program, Instituto Mexicano del Petróleo, México

Received: June 19, 2002

A molecular theory to determine thermodynamic properties of isotropic and nematic phases of liquid crystals is proposed, based on a "convex peg" model and semiempirical PM3 (Parametrized Method 3) calculations. The Helmholtz-free energy of the molecular system, a convex hard core within an encircling spherical square-well (SW) potential, is obtained from a second-order perturbation theory for SW nonspherical particles, combined with the Parsons decoupling approximation of the translational and rotational degrees of freedom, and a long-range approximation for the evaluation of the perturbation terms. The theory is applied to predict the phase diagram and isotropic−nematic transition of *p*-azoxyanisole. To do this, an estimation of the volume of a *p*-azoxyanisole molecule is derived from a minimum-energy geometry, using PM3 calculations; the volume obtained is mapped into a hard ellipsoid revolution volume of a Convex Peg molecule. A very good agreement in the prediction of the thermodynamic properties is obtained when compared with experimental data.

1. Introduction

Over the past two decades, computer simulation studies[1−4] of anisotropic hard-core molecular models have confirmed that anisotropy in the shape of molecules is the essential feature for liquid crystal phase behavior, as Onsager demonstrated theoretically using a virial expansion for a fluid formed by long rods.[5] From computer simulation studies, we know now that, for example, hard ellipsoids of revolution[2] (HER) fluids exhibit a nematic liquid crystal phase for elongations greater than 2.75:1, and a hard spherocylinder (HSC) system[3,4] has a nematic phase for aspect ratios greater than 4. The Onsager theory is exact in the limit of infinitely long rods, and although it is quantitatively deficient for rods of intermediate elongation, it is a molecular-based theory and thus can be improved systematically. One possible route to improve the Onsager theory is by including higher virial coefficients.[6]

A very useful and simple approach that extends the application of the Onsager theory to finite length rods is the decoupling approximation of translational and orientational degrees of freedom, proposed by Parsons.[6,7] This approximation has been extensively used in theoretical studies of thermodynamic and structural predictions for isotropic and nematic phases,[4,8−10] leading to a very good prediction of the I−N phase transition for convex molecular geometries. The Parsons approach takes advantage of accurate and analytical results valid for a hard spheres (HS) fluid (such as the Carnahan and Starling equation of state[11] and the Percus−Yevick[12] direct correlation function) to extend its validity to nematic phases and basically consists of scaling the distance between nonspherical particles by the distance of nearest approach at the same relative orientation.

Because real molecules also have attractive interactions, such as the van der Waals forces, a thermodynamic molecular approach must take into account their description for a proper prediction of the phase diagram. In the Maier−Saupe theory,[13] the attractive energy arising from induced dipolar moments is given by a mean-field approximation, to predict their effect in the I−N phase transition. Although Maier−Saupe and Onsager theories model different molecular effects, they are complementary theories that can be combined to give a first approach to theoretical equations of state for liquid crystalline systems, as the Augmented van der Waals theory (AVDW)[14] does for isotropic fluids.

After the success of perturbation theories in describing liquid isotropic phases, several mean-field theories[15−18] have been proposed that basically extend the AVDW approach to nonisotropic fluids. Recently, Williamson[19] extended the first-order Barker and Henderson perturbation theory[20] for isotropic fluids to model a convex peg molecule, using the Parsons approach,[7] and a long-range approximation (BHLR)[21] for the calculation of the first perturbation term. The convex peg model comprises a convex hard-core molecule within an encircling spherical square-well potential (SW); see Figure 1. Although the convex peg model uses an isotropically attractive interaction, the nonspherical hard-core introduces an effective anisotropy in the attractive forces. Gelbart and Gelbart[22] demonstrated that molecular models comprised of an anisotropic core plus isotropically attractive interactions give the basic orientational behavior in nematics, and that most of the anisotropic interaction in these phases results from the coupling between the anisotropic

* To whom correspondence should be addressed. E-mail: richa@quijote.ugto.mx.
† Facultad de Química, Universidad de Guanajuato.
‡ Instituto de Física, Universidad de Guanajuato.
§ Molecular Engineering Program, Instituto Mexicano del Petróleo.

10.1021/jp021453o CCC: $22.00
Published on Web 09/26/2002

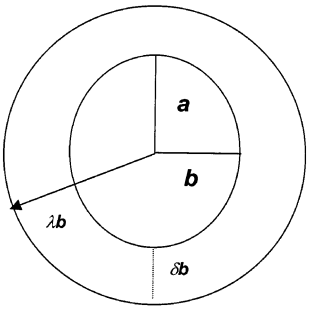

Figure 1. Convex Peg model comprising a convex hard core with semi-axis ratio *a:b* surrounded by a spherical square-well of depth ϵ and range λb. The square-well extends beyond the tips of the convex core to a distance δ.

repulsion and the isotropic attraction. Evans and co-workers[23,24] have examined the phase diagram of the convex peg model using an AVDW theory, i.e., the hard core is treated as accurately as possible and the contributions from the attractive forces are incorporated using the second virial coeffcient[24] and its high-temperature limit.[23] These theories give the general features of the phase diagram and qualitatively agree with the simulation data reported by de Miguel and Allen.[25]

For SW spherical particles, the first-order BH-LR theory improves the AVDW approach in two and three dimensions.[26−28] Its extension to anisotropic fluids[19] agrees accurately with simulation data for fluids of prolate uniaxial cores 3:1, including the I−N phase transition. In this paper, the theory presented in ref 19 is extended to second-order and used to predict the phase diagram of a real molecule. The second-order perturbation theory is obtained using the local compressibility approximation (LCA) proposed by Barker and Henderson[29] for SW spherical fluids. Although the LCA gives only a very approximated description of the second-order contribution to the Helmholtz free-energy for SW systems,[30] it provides a compact analytical expression that can be used to assess the effect of this term in the prediction of phase diagrams of liquid crystals. By means of quantum mechanical calculation, an estimated value of the p-azoxyanisol volume was derived. We present in section 4 the application of the theory to characterize the I−N phase diagram of this compound.

2. Molecular Thermodynamic Theory for a Liquid Crystal

We consider a one-component fluid composed of N molecules, hard ellipsoids of revolution (HER) with semimajor axis a and semiminor axis b, contained within a volume V at a temperature T. The molecules interact via a square-well potential

$$u(r_{ij};\Omega_i,\Omega_j) = \begin{cases} \infty & r_{ij} \in V_{ex}(\Omega_i,\Omega_j) \\ -\epsilon & r_{ij} \le \lambda\sigma \\ 0 & r_{ij} > \lambda\sigma \end{cases} \quad (1)$$

where r_{ij} is the distance between the center of mass for particles i and j with orientational coordinates Ω_i and Ω_j, respectively, $V_{ex}(\Omega_i,\Omega_j)$ is the excluded volume that depends on the orientations of the particles, $\sigma = 2b$ is the diameter of a sphere centered at the particle's center of mass, $\lambda\sigma$ is the range of the square-well ($\lambda\sigma = 2a + \delta\sigma$, where $\delta\sigma$ is the distance between the edge of the square well and the ends of the spherocylinder, as shown in Figure 1), and ϵ is the SW depth. The SW potential given in eq 1 belongs to the general class of hard-core potentials given by $u(12) = u_0(12) + \epsilon u_p(12)$, which consists of a repulsive hard-core term $u_0(1,2)$ plus an attractive interaction $\epsilon u_p(1,2)$; for the SW interaction the last term reduces to the step function. A system of particles interacting via this type of potentials can be treated by a perturbation approach to obtain the Helmholtz free-energy A, using the hard-core system as the reference fluid. Following Barker and Henderson,[20,29] and Williamson,[19] A is given by a high-temperature expansion (HTE), that in our case we will approximate to second order

$$\frac{A}{NkT} = \frac{A_{ideal}}{NkT} + \frac{A_\Omega}{NkT} + \frac{A_0}{NkT} + \frac{a_1}{T^*} + \frac{a_2}{T^{*2}} \quad (2)$$

Here, A_{ideal} is the ideal contribution to the free energy, A_Ω is an orientational free energy, A_0 is the Helmoltz free energy of the reference fluid, a_1 and a_2 are the first and second-order perturbation terms, and $T^* = kT/\epsilon$ is a scaled temperature, where k is the Boltzmann's constant.

The ideal term is given by

$$\frac{A_{ideal}}{NkT} = \ln(\rho\Gamma) - 1 \quad (3)$$

where Γ is a volume parameter determined by the molecular degrees of freedom. Taking into account traslational and rotational degrees of freedom, we have that $\Gamma = \Lambda^3 c$, where Λ is the de Broglie's wavelength, and c is a rotational constant given by $c = h^2/8\pi^2 IkT$, I being the molecular moment of inertia.

The orientational term arises from a loss of entropy when orientational order is present, and is given by the Onsager's expression

$$\frac{A_\Omega}{NkT} = \int f(\Omega) \ln[4\pi f(\Omega)]\, d\Omega \quad (4)$$

where $f(\Omega)$ is the single particle orientational distribution function (SPODF) for a solid angle Ω, that satisfies the normalization condition $\int f(\Omega)\, d\Omega = 1$. For an isotropic phase, $f(\Omega) = 1/4\pi$, whereas for a nematic phase the SPODF is a nonuniform function.

The hard-core free energy A_0 is given by the Lee−Parsons expression[7−9]

$$\frac{A_0}{NkT} = \frac{\langle V_{ex}(\Omega_1,\Omega_2)\rangle_{\Omega_1,\Omega_2}}{8V_m}\frac{A_{HS}}{NkT} \quad (5)$$

In this equation, V_m is the volume of the hard core, A_{HS} is the Helmholtz free energy of a hard spheres fluid with the same packing fraction of the hard-core fluid, i.e., $\eta = \rho V_m$, and $\langle V_{ex}(\Omega_1,\Omega_2)\rangle_{\Omega_1,\Omega_2}$ is the angular average of the excluded volume between two particles, that can be expressed as

$$\langle V_{ex}(\Omega_1,\Omega_2)\rangle_{\Omega_1,\Omega_2} = -\frac{1}{V}\iint (e^{-u_0(12)/kT} - 1)\, f(\Omega_1)\, f(\Omega_2)\, d1\, d2$$

$$= -4\pi\iiint_0^\infty (e^{-u_0(12)/kT} - 1) r_{12}^2 f(\Omega_1) \times f(\Omega_2)\, dr_{12}\, d\Omega_1\, d\Omega_2 \quad (6)$$

The averaged excluded volume in eq 6 is written in terms of the Mayer function for the binary repulsive interaction, i.e., $F(12) = e^{-u_0(12)/kT} - 1$, with the values $F(12) = -1$ and $F(12) = 0$ for overlapping and non overlapping particles, respectively.

Introducing these values of the Mayer function enable us to rewrite eq 6 in terms of the collision diameter between two particles, $s(\Omega_1,\Omega_2)$

$$\langle V_{ex}(\Omega_1,\Omega_2)\rangle_{\Omega_1,\Omega_2} = 4\pi\iiint_0^{s(\Omega_1,\Omega_2)} r_{12}^2 f(\Omega_1)\, f(\Omega_2)\, dr_{12}\, d\Omega_1\, d\Omega_2 \quad (7)$$

The perturbation terms a_1 and a_2 give the thermodynamic contribution due to attractive forces. The first-order term is a mean attractive energy given by

$$a_1 = \frac{\rho}{2V}\iint u_p(12)\, g_0(12)\, d1\, d2 = -2\pi\rho\iiint_s^{\lambda\sigma} g_0(12)\, f(\Omega_1)\, f(\Omega_2) r_{12}^2\, dr_{12}\, d\Omega_1\, d\Omega_2 \quad (8)$$

whereas the second-order term gives a first estimation of fluctuations of the attractive energy with respect to its mean value, and that in the LCA approximation is given by

$$a_2 = -\frac{\rho}{2}\frac{\partial}{\partial P}\{2\pi\rho\iiint_s^{\lambda\sigma}[u_p(12)]^2 \times g_0(12)\, f(\Omega_1)\, f(\Omega_2) r_{12}^2\, dr_{12}\, d\Omega_1\, d\Omega_2\} = -K_0\frac{\rho}{2}\frac{\partial a_1}{\partial \rho} \quad (9)$$

where P is the pressure of the fluid and K_0 gives the isothermal compressibility for the repulsive hard-core fluid. In these equations, $g_0(12)$ is the pair distribution function of the hard-core reference fluid, which depends on the orientational and positional coordinates of two molecules.

The perturbation terms given in eqs 8 and 9 can be also expressed in terms of the total correlation function $h_0(12)$, defined by $h_0(12) = g_0(12) - 1$. This allows us to study the perturbation terms a_1 and a_2 as functions of the SW range λ in a systematic way, as del Río and co-workers have shown for isotropic SW fluids in a series of studies.[26−28,30−32] The extension of the same approach to anisotropic SW systems is straightforward, but here we will focus the attention to a_1 only because the analysis for a_2 is algebraically more complex.[30]

Because $g_0(12)$ is null inside the core, i.e., $r_{12} < s(\Omega_1,\Omega_2)$, then the lower limit of the positional integral in eq 7 can be changed to zero without modifying the actual value of a_1

$$a_1 = -2\pi\rho\iiint_0^{\lambda\sigma} g_0(12)\, f(\Omega_1)\, f(\Omega_2) r_{12}^2\, dr_{12}\, d\Omega_1\, d\Omega_2$$

and by introducing the definition of $h_0(12)$, we have

$$a_1 = -2\pi\rho\iiint_0^{\lambda\sigma}[h_0(12)+1] f(\Omega_1)\, f(\Omega_2) r_{12}^2\, dr_{12}\, d\Omega_1\, d\Omega_2$$

which can be partially integrated and expressed as

$$a_1 = -\frac{2\pi\rho^*\lambda^3}{3} - 2\pi\rho^*\iiint_0^{\lambda} h_0(12)\, f(\Omega_1)\, f(\Omega_2) x^2\, dx\, d\Omega_1\, d\Omega_2 \quad (10)$$

where the reduced variables $\rho^* = \rho\sigma^3$ and $x = r/\sigma$ are used. The second term in eq 10 can be split in two integrals by changing the integration domains

$$\iiint_0^{\lambda} h_0(12)\, f(\Omega_1)\, f(\Omega_2) x^2\, dx\, d\Omega_1\, d\Omega_2 = \iiint_0^{\infty} h_0(12)\, f(\Omega_1)\, f(\Omega_2) x^2\, dx\, d\Omega_1\, d\Omega_2 - \iiint_{\lambda}^{\infty} h_0(12)\, f(\Omega_1)\, f(\Omega_2) x^2\, dx\, d\Omega_1\, d\Omega_2 \quad (11)$$

Equation 11 is useful because it allows us to introduce the definition of K_0, a thermodynamic property of the hard-core reference fluid

$$K_0 = kT\left(\frac{\partial\rho}{\partial P_0}\right) = 1 + 4\pi\rho^*\iiint_0^{\infty} h_0(12)\, f(\Omega_1)\, f(\Omega_2) x^2\, dx\, d\Omega_1\, d\Omega_2 \quad (12)$$

Using eqs 11 and 12, the attractive energy given in eq 10 can be finally expressed as

$$a_1 = -\frac{2\pi\rho^*\lambda^3}{3} + \left(\frac{1-K_0}{2}\right) + 2\pi\rho^*\iiint_{\lambda}^{\infty} h_0(12)\, f(\Omega_1)\, f(\Omega_2) x^2\, dx\, d\Omega_1\, d\Omega_2 \quad (13)$$

The first term in eq 13 is the van der Waals contribution to a_1 and is dominant for large λ. The second term is independent of λ and is the first correction to the van der Waals approximation. The last term is a correction important for λ close to 1, and for isotropic SW fluids it results a complicated function of η and λ that tends to zero as λ increases[31] because $h_0(12)$ goes to zero as the distance is increased. The long-range approximation (LRA)[21,31] is then given by neglecting this last term, and that describes accurately 2D and 3D SW isotropic fluids.[26−28] Because the LCA approximation for a_2 is given as the derivative of a_1 with respect to density, it is clear that the complete thermodynamic contribution of the perturbation terms is given by a_1 and the isothermal compressibility factor K_0, i.e.

$$a_1 = -\frac{2\pi\rho^*\lambda^3}{3} + \left(\frac{1-K_0}{2}\right) \quad (14)$$

$$a_2 = -K_0\frac{\rho^*}{2}\frac{\partial a_1}{\partial \rho^*} \quad (15)$$

Equations 2−5, 14, and 15 resume the LRA−MCA perturbation theory for the convex peg model, that can be applied if the compressibility factor of the hard-core reference fluid, K_0, is known. However, if this is not the case, then the decoupling approximation of Parsons can be used. For doing this, notice that in eq 6 we can use the collision diameter $s(\Omega_1,\Omega_2)$ to scale the relative distance between two particles, i.e., we introduce the variable $z = r_{12}/s(\Omega_1,\Omega_2)$ in eq 6 to obtain the following expression

$$\langle V_{ex}(\Omega_1,\Omega_2)\rangle_{\Omega_1,\Omega_2} = 4\pi\iiint_0^1 z^2\, dz\, s^3(\Omega_1,\Omega_2)\, f(\Omega_1)\, f(\Omega_2)\, d\Omega_1\, d\Omega_2 \quad (16)$$

and because the integral in z can be performed directly, we obtain a simple relation

$$\langle V_{ex}(\Omega_1,\Omega_2)\rangle_{\Omega_1,\Omega_2} = \frac{4\pi}{3}\iint s^3(\Omega_1,\Omega_2)\, f(\Omega_1)\, f(\Omega_2)\, d\Omega_1\, d\Omega_2 \quad (17)$$

or equivalently

$$\langle V_{ex}(\Omega_1,\Omega_2)\rangle_{\Omega_1,\Omega_2} = \left\langle \frac{4\pi}{3} s^3(\Omega_1,\Omega_2)\right\rangle_{\Omega_1,\Omega_2} \quad (18)$$

that states that the angular average of the excluded volume of two nonspherical particles is equivalent to the volume of a sphere whose diameter is the angular average of the collision diameter between the particles. The scaling argument used here to obtain eq 18 from eq 6 is the essence of the Parson approach, and can be applied also to eq 12, to relate the isothermal compressibility factors K_0 and K_{HS}, the last one corresponding to a fluid of hard spheres of diameter $\langle s(\Omega_1,\Omega_2)\rangle_{\Omega_1,\Omega_2}$.

Introducing the scaled variable z in eq 12, and following the same arguments used to obtain eq 18, we have that

$$K_0 = 1 + 4\pi\rho \iiint_0^\infty h_0(z) z^2\, dz\, s^3(\Omega_1,\Omega_2)\, f(\Omega_1)\, f(\Omega_2)\, d\Omega_1\, d\Omega_2$$

$$= 1 + 4\pi\rho \int_0^\infty h_0(z) z^2\, dz \iint s^3(\Omega_1,\Omega_2)\, f(\Omega_1) \times f(\Omega_2)\, d\Omega_1\, d\Omega_2 \quad (19)$$

and identifying in the second line of this equation the expression of the angular average of the excluded volume, eq 17, we have that

$$K_0 = 1 + 3\langle V_{ex}(\Omega_1,\Omega_2)\rangle_{\Omega_1,\Omega_2}\rho \int_0^\infty h_0(z) z^2\, dz \quad (20)$$

The isothermal compressibility factor K_{HS} is obtained from eq 12 for spherical particles

$$K_{HS} = kT\left(\frac{\partial\rho}{\partial P_{HS}}\right) = 1 + 4\pi\rho^* \int_0^\infty h_{HS}(x) x^2\, dx \quad (21)$$

Then, if we use the approximation $h_0(z) = h_{HS}(z)$ in eq 20, from eq 21 we have that eq 20 can be approximated by

$$K_0 = 1 + \frac{3}{4\pi\sigma^3}\langle V_{ex}(\Omega_1,\Omega_2)\rangle_{\Omega_1,\Omega_2}(K_{HS} - 1) \quad (22)$$

which is the desired relation that we were looking for, because it allows us to calculate the isothermal compressibility of the anisotropic hard-core fluid through K_{HS}. Using the decoupling result of eq 20 in eqs 14 and 15, we have finally then the following LRA−MCA−Parsons perturbation terms

$$a_1 = -\left[4\eta\lambda^3 + \frac{\langle V_{ex}(\Omega_1,\Omega_2)\rangle_{\Omega_1,\Omega_2}}{16V_m}(K_{HS} - 1)\right]\left(\frac{b}{a}\right) \quad (23)$$

$$a_2 = -\left(1 + \frac{\langle V_{ex}(\Omega_1,\Omega_2)\rangle_{\Omega_1,\Omega_2}}{8V_m}(K_{HS} - 1)\left(\frac{b}{a}\right)\right)\frac{\eta}{2}\frac{\partial a_1}{\partial\eta} \quad (24)$$

where $V_m = {}^4/_3\pi ab^2$ and $\sigma = 2b$. Equations 14 and 15 reduce to the perturbation expressions for an isotropic SW fluid when $a = b$, because in this case $\langle V_{ex}(\Omega_1,\Omega_2)\rangle_{\Omega_1,\Omega_2} = 8V_m$.

In summary, by collecting the different contributions to the free energy obtained before (eqs 3−5, 23 and 24), we arrive to the following expression for the Helmholtz free-energy in the LRA−MCA. Parsons approximations

$$\frac{A}{NkT} = \ln(\rho\Gamma) - 1 + \int f(\Omega)\ln[4\pi f(\Omega)]\, d\Omega + \Psi\frac{A_{HS}}{NkT} - 4\omega\beta\eta\lambda^3 - \Psi\omega\left(\beta + \beta^2\eta\frac{\partial a_1}{\partial\eta}\right)\frac{(K_{HS} - 1)}{2} - \frac{\beta^2}{2}\eta\frac{\partial a_1}{\partial\eta} \quad (25)$$

where $\beta = 1/T^*$, $\omega = b/a$, and $\Psi = \langle V_{ex}(\Omega_1,\Omega_2)\rangle_{\Omega_1,\Omega_2}/8V_m$. To be able to use this expression, we need to know the HS thermodynamic properties A_{HS} and K_{HS}, and the excluded volume $\langle V_{ex}(\Omega_1,\Omega_2)\rangle_{\Omega_1,\Omega_2}$. For the HS properties, we use the Carnahan−Starling equation of state,[11] thus

$$\frac{A_{HS}}{NkT} = \frac{4\eta - 3\eta^2}{(1-\eta)^2} \quad (26)$$

$$K_{HS} = \frac{(1-\eta)^4}{1 + 4\eta + 4\eta^2 - 4\eta^3 + \eta^4} \quad (27)$$

whereas $\langle V_{ex}(\Omega_1,\Omega_2)\rangle_{\Omega_1,\Omega_2}$ is calculated from the exact angular dependent excluded volume $V_{ex}(\Omega_1,\Omega_2)$, using the recipe of Camp et al.,[10] which gives a reliable description of the thermodynamic properties of both the isotropic and nematic phases of a hard-core fluid.[4,19,33]

In the isotropic phase, the free energy is obtained from eq 25 with $f(\Omega_i) = 1/4\pi$, $i = 1, 2$ that corresponds to a uniform distribution of molecular orientations. In the case of the nematic phase, we have to consider eq 25 as a free energy functional of $f(\Omega)$, which must be minimized with respect to this function. For this work, we have used a numerical minimization using the Onsager's trial function

$$f(\Omega) = \frac{\alpha\cosh(\alpha\cos\theta)}{4\pi\sinh\alpha} \quad (28)$$

where α is a variable parameter.

Once we have obtained the free energies for the isotropic and nematic phases, the pressure P and chemical potential μ can be evaluated from the standard thermodynamic relationships

$$P = -\left(\frac{\partial A}{\partial V}\right)_{T,N} \quad (29)$$

$$\mu = -\left(\frac{\partial A}{\partial N}\right)_{T,V} \quad (30)$$

The phase diagram is studied using eqs 29 and 30 and by ensuring for a fixed temperature that the chemical potential and pressure of each phase are the same.

3. Molecular Volume

Application of quantum theory to chemical systems allows the calculation of molecular parameters. Quantum mechanical calculations are based on the minimization of the total energy of the molecule with respect to all or some structural parameters. The optimization procedure lead to the most stable structure observed in ideal conditions.

Molecular parameters obtained by molecular modeling procedures depend on the method followed to solve the Schröedinger equation: molecular mechanics, ab initio, semiempirical methods, etc.[34] Semiempirical methods start with the same two approximations inherent to ab initio methods, and make use of a minimal valence basis of Slater Type Orbitals (STOs). The central assumption in these methods is the NDDO (neglect of diatomic differential overlap) approximation, which implies that two functions do not overlap unless they are located

TABLE 1: Temperature $T^* = kT/\epsilon$, Coexisting Packing Fractions $\eta = NV_m/V$, Density Jump $\Delta\eta = \eta_{nem} - \eta_{iso}$ and Pressure $P^* = PV_m/kT$ at the I−N Phase Transition for a "Convex Peg" Fluid with a Prolate Ellipsoid Hard Core 3:1 and $\delta = 0$

T^*	η_{iso}	η_{nem}	$\Delta\eta$	P^*
∞	0.566	0.574	0.008	15.941
2.8	0.561	0.570	0.009	11.137
2.6	0.560	0.570	0.009	10.777
2.4	0.560	0.569	0.009	10.359
2.2	0.559	0.569	0.010	9.866
2.0	0.558	0.569	0.010	9.275
1.8	0.557	0.568	0.010	8.569
1.6	0.556	0.567	0.011	7.684
1.4	0.555	0.566	0.011	6.567
1.2	0.553	0.565	0.012	5.106
1.0	0.550	0.564	0.014	3.082
0.9	0.548	0.563	0.015	1.755
0.89	0.548	0.563	0.015	1.610
0.88	0.547	0.563	0.016	1.462
0.87	0.547	0.563	0.016	1.309
0.86	0.547	0.563	0.016	1.152
0.85	0.546	0.563	0.016	0.993
0.84	0.546	0.563	0.016	0.831
0.83	0.546	0.562	0.016	0.665
0.82	0.546	0.562	0.017	0.495
0.81	0.545	0.562	0.017	0.321
0.80	0.545	0.562	0.017	0.144
0.795	0.545	0.562	0.018	0.054
0.794	0.545	0.562	0.018	0.036
0.793	0.545	0.562	0.018	0.017
0.792	0.000	0.562	0.562	0.000
0.750	0.000	0.577	0.577	0.000
0.700	0.000	0.592	0.592	0.000
0.650	0.000	0.606	0.606	0.000

on the same atomic centers, i.e., $\int \phi_\mu \phi_\nu \, d\tau = 0$ for μ and ν not on the same center. This leads to a set of equations similar to the Roothaan−Hall equations but with a greatly simplified Fock matrix. One important feature of semiempirical methods is that they are applicable to fairly large organic molecules containing 200 or more atoms.

Semiempirical methods yields continuous energy surfaces from which parameters such as the molecular volume can be derived. In this work, an optimization of the electronic structure and geometry by PM3 semiempirical molecular orbital calculations[35] has been carried out. Molecular characteristics for PAA corresponds to the energy minima obtained by geometry optimization and a full degree of freedom analysis was made using the gradient optimization routine in the programs. All calculations were carried out on a Silicon Graphics Octane Workstation (Dual MIPS RISC R10000 64-bit 195 MHz/1MB cache Processor, IRIX 6.4 operating system, 256 MB RAM, 4 GB Disk). We used the Gaussian 94 program and prepared molecular coordinates inputs with Spartan 5.1.1 program. The molecular volume obtained by this method represents a isodensity surface, and was derived considering an electron density of 0.08 electrons/Å^3. This volume is essentially similar to the volume that encloses the electron density derived from the overlapping of molecular orbitals that occur during bond formation. We used the volume derived from the electronic density of the molecule to map an ideal molecular volume, and treated it as equivalent to the HER volume described above.

4. Results and Discussion

The phase diagrams of ellipsoidal hard-cores of ratios $a/b = 3$, 3.1, and 3.5, with a spherical square-well with $\delta = 0$, were examined using the perturbation theory discussed in section 2. Results are given in Tables 1 and 2 for the systems $a/b = 3$ and 3.5, respectively, and in Figure 2 for the system $a/b = 3.1$. Because the theory describes isotropic and nematic phases only, positionally ordered phases cannot be predicted. Qualitatively, the general features observed in these results agree with those reported by Tjipto−Margo and Evans[23] and García et al.:[36] there is a critical temperature T_c, with vapor and liquid phases for temperatures below T_c, and an isotropic homogeneous fluid phase above T_c; a nematic phase arises at higher densities, with a very well-defined isotropic−nematic transition, and with decreasing temperature, a vapor−liquid−nematic (V−L−N) triple-point T_T appears where these three phases coexist; below T_T, the liquid phase disappears and only the vapor and nematic phases coexist. For a different potential, using a mean-field approach, Telo da Gama[37,38] predicts a similar phase diagram. From the limited simulation data reported in the literature, the LRA−MCA Parsons theory provides a good description for the

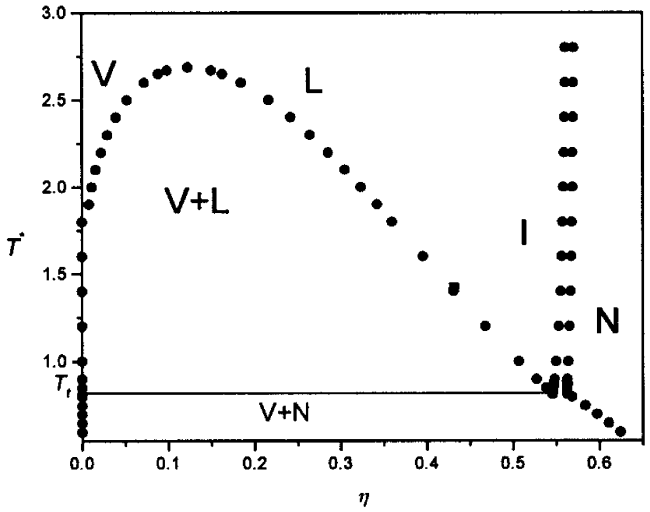

Figure 2. Partial phase diagram ($T^* - \eta$ slice) for a convex peg fluid with prolate ellipsoid hard core 3:1 and $\delta = 0$ obtained from PT.

TABLE 2: Temperature $T^* = kT/\epsilon$, Coexisting Packing Fractions $\eta = NV_m/V$, Density Jump $\Delta\eta = \eta_{nem} - \eta_{iso}$ and Pressure $P^* = PV_m/kT$ at the I−N Phase Transition for a "Convex Peg" Fluid with a Prolate Ellipsoid Hard Core 3.5:1 and $\delta = 0$

T^*	η_{iso}	η_{nem}	$\Delta\eta$	P^*
∞	0.509	0.522	0.012	10.278
2.8	0.501	0.519	0.017	5.205
2.7	0.500	0.518	0.017	5.000
2.5	0.499	0.518	0.018	4.605
2.3	0.498	0.518	0.019	4.135
2.1	0.497	0.517	0.020	3.572
1.9	0.496	0.517	0.021	2.905
1.7	0.494	0.517	0.023	2.088
1.5	0.492	0.517	0.026	1.069
1.4	0.490	0.518	0.028	0.458
1.39	0.490	0.518	0.028	0.394
1.38	0.489	0.518	0.029	0.326
1.37	0.489	0.518	0.029	0.259
1.36	0.489	0.518	0.029	0.191
1.35	0.489	0.518	0.030	0.122
1.34	0.488	0.519	0.030	0.052
1.335	0.488	0.519	0.030	0.016
1.334	0.488	0.519	0.030	0.009
1.333	0.488	0.519	0.030	0.002
1.332	0.000	0.519	0.519	0.000
1.3	0.000	0.527	0.527	0.000
1.2	0.000	0.548	0.548	0.000
1.1	0.000	0.567	0.567	0.000
1.0	0.000	0.586	0.586	0.000
0.9	0.000	0.605	0.605	0.000
0.8	0.000	0.625	0.625	0.000

TABLE 3: Comparison of Various Parameters Obtained Experimentally at the I−N Phase Transition at 1 atm Pressure and a Temperature of 409 K for PAA with the Theoretical Prediction from VDW Theory and PT

property	expt (PAA) (ref 41)	(this work) (3.5:1)	(this work) (3:1)	BH−PT (ref 19) (3:1)	HTE (ref 23) (3:1.4:1)	HTE (ref 23) (3:1.45:1)
V_m (Å^3)		70	230	230	230	230
ϵ/k (K)		307	515.8	486	695	738
$(T\,(\mathrm{K}))_{1\ \mathrm{atm}}$	409	409	409	408.8	406	411
η	0.62	0.519	0.562	0.548	0.523	0.523
$\Delta\eta/\eta$	0.0035	0.057	0.032	0.025	0.015	0.012
$\langle P_2\rangle$	0.36	0.69	0.63	0.57	0.40	0.36
$\langle P_4\rangle$	0.07	0.30	0.22	0.23	0.11	0.09
$\Delta S/Nk$	0.17	1.07	0.80	0.67	0.23	0.23

thermodynamic properties of the prolate convex-peg fluid with $\lambda \geq 3$.

However, there are two major limitations of the theory that deserve special attention. First, because liquid-state molecular theories valid only for isotropic and nonisotropic fluids cannot predict phases with positional order (Smectic (Sm) or Crystalline (K)), the V−L−N triple point in Figure 2 could be preempted by a V−L−Sm or V−L−K triple point. This must be stressed because the triple point predicted by our theory occurs at zero pressure. In consequence, the predicted results given for the I−N phase transition near to the triple point could not be realistic and must be taken with reserves. Second, we must proceed with caution extrapolating a perturbation theory beyond its range of validity because the equation of state given by eq 25 is based on a second-order high-temperature expansion, and then it will fail at low temperatures. Although the low-temperature limit where eq 25 is still valid requires a more detailed study, Benavides et al.[30,32] have demonstrated for SW spherical fluids that a second-order HTE equation of state in the long-range approximation becomes inaccurate when the temperature is of the order of $0.6T_c$. We should conclude that the prediction given near the I−L−N triple point in Figure 2 is approximated because $T_T \approx 0.3T_c$. It is clear then that these limitations of the theory restrict the validity of the predictions obtained in the low-temperature region of the phase diagram.

Several studies have focused the attention in describing the phase diagram of 4,4′-dimethoxyazoxybenzene (*p*-azoxyanisole, PAA), which presents an I−N transition at 1 atm pressure.[19,23,39,40] For example, Tjipto-Margo and Evans[23] predicted the phase diagram for this compound using a HTE VDW theory for two biaxial cores, 3:1.4:1 and 3:1.45:1 with $\delta = 0$, and determined the molecular parameters through a fitting procedure consisting in to fix the value of the molecular volume to 230 Å^3, and then fitting the potential well depth ϵ to reproduce the I−N transition temperature at 1 atm. Williamson[19] used the same approach with a first-order HTE EOS for an uniaxial core 3:1 and $\delta = 0$, but the pressure−temperature behavior prediction in the I−N phase transition around 1 atm results to be poor.

We studied the PAA phase diagram with eq 25 using the approach of Tjipto−Margo and Evans[23] already explained. The results are reported in Table 3. Because the reduced pressure PV_m/ϵ has a linear dependence with T^*, the fitting procedure is straightforward. The I−N transition temperatures predicted in this way can be compared with experimental data (taken from Chandrasekhar[41]) over a wide range of pressures, as indicated in Figure 3 (solid line). The theoretical prediction obtained is clearly very poor. Results cannot be improved with different fitting values; for example, the short dot line in Figure 3 corresponds to a fitting at zero pressure and for a temperature of 407 K.

The predictions can be improved if we consider the molecular geometry for PAA derived from more accurate quantum mechanical methods, such as the PM3 method.[35] This approach

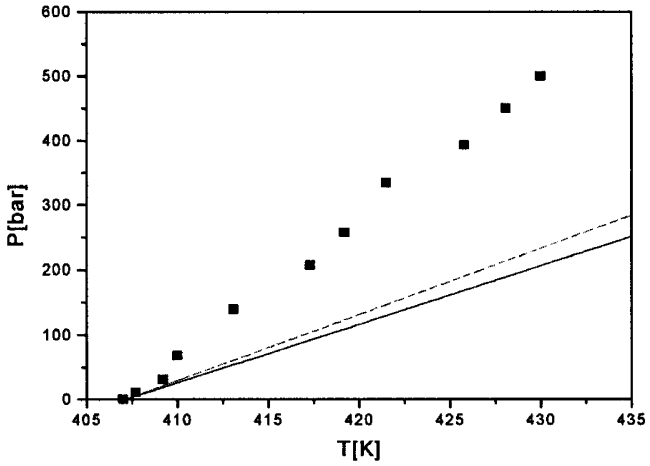

Figure 3. Pressure (in bar) plotted as a function of the temperature (in K) at the I−N phase transition for the nematogen PAA. The solid line represents the theoretical prediction of PT (3:1 core with $\delta = 0$) fitted at 1 atm and 409 K. The short dot line represents the predictions from the same theory fitted at zero pressure and 407 K and the boxes represent the experimental data taken from Chandrasekhar.[41]

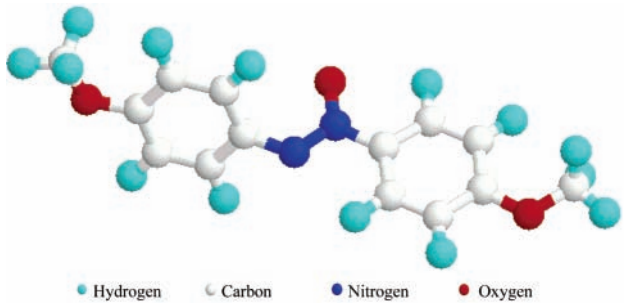

Figure 4. Minimum-energy geometry for p-azoxyanisole or 4,4′-dimethoxyazoxybenzene ($CH_3OC_6H_4NONC_6H_4OCH_3$, PAA) obtained by PM3 method.[35]

is used to find three bond lengths: $2a$ is taken as the distance between hydrogens of the methoxy groups localized in the extremes of the PAA molecule, b is the distance between nitrogen (N_1) and oxygen (O_3) of the azoxy group ($N_1{=}N_2{-}O_3$) at the center of the molecule, and $2c$ is the distance between hydrogens on the meta position in the benzene ring (see Figure 4). The PM3 values obtained are $a = 7.60$ Å, $b = 2.17$ Å, and $c = 2.15$ Å, then $a/b \approx 3.5$, and the corresponding molecular volume is 70 Å^3. Notice that the molecular volume obtained by the PM3 method is considerably smaller than the fitted values reported previously, and its effect on the thermodynamic prediction is not negligible at all.

To implement the mapping of the PM3 volume into the HER molecular geometry to be used in the thermodynamic perturbation theory, we choose to keep the PM3 values of the molecular volume and the aspect ratio a/b, which are the only parameters

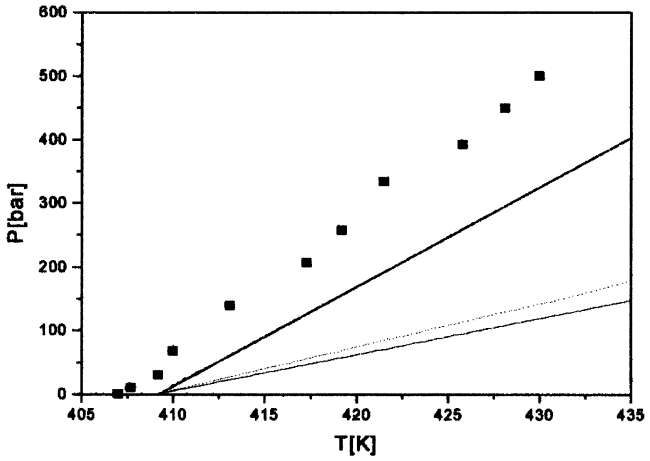

Figure 5. Pressure (in bar) plotted as a function of the temperature (in K) at the I−N phase transition for the nematogen PAA. The lower solid line represents the theoretical prediction of PT (3.5:1 core with $\delta = 0$) fitted at 1 atm, $V_m = 230$ Å^3 and 409 K. The short dot line represents the prediction from the same theory fitted at zero pressure and volume, but with 407 K. The upper solid line represents the prediction from the same theory fitted at 1 atm, $V_m = 70$ Å^3 and 409 K and the boxes represent the experimental data taken from Chandrasekhar.[41]

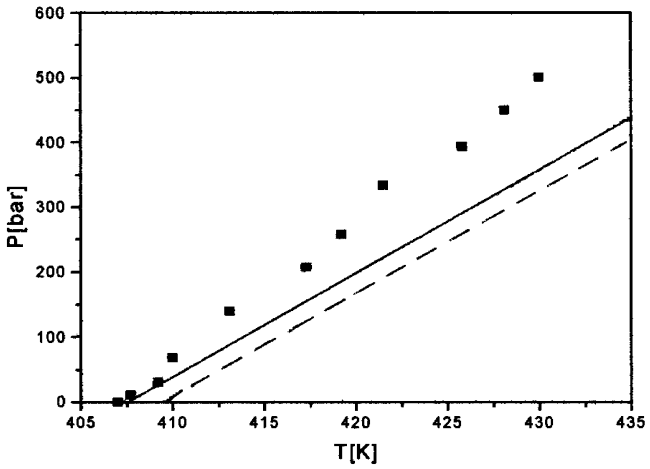

Figure 6. Pressure (in bar) plotted as a function of the temperature (in K) at the I−N phase transition for the nematogen PAA. The solid line represents the theoretical prediction of PT (3.5:1 core with $\delta = 0$) fitted at 1 atm, $V_m = 70$ Å^3 and 409 K. The dashed line represents the prediction from the same theory fitted at 1 atm, $V_m = 70$ Å^3 and 407 K and the boxes represent the experimental data taken from Chandrasekhar.[41]

required for the calculation of the thermodynamic properties, as can be seen in eq 25. The mapped HER molecule with volume of 70 Å^3 has semi-axes $c' = b'$ and $a' = 3.5b'$, i.e., $a' = 5.88$ Å and $b' = 1.68$ Å, but the reader must bare in mind that the values that are relevant for the theory are not the axes lengths but the molecular aspect ratio and the molecular volume. The PM3 molecular volume is used to determine the potential well depth ϵ by reproducing the I−N temperature transition $T = 409\ K$ for $P = 1$ atm. In Figure 5 we report the prediction obtained in this way (solid line), which is compared with the other two predictions already explained above. We observe that a considerable improvement in the prediction is obtained. If we readjust the values to reproduce the conditions $T = 407\ K$ for $P = 0$ atm, then a better agreement is observed with the experimental data (see solid line Figure 6). We can conclude that a more accurate method for the calculation of the molecular volume, as obtained here using a quantum mechanical method, can improve the thermodynamic prediction. This approach is quite different from a simple refitting procedure. On the other hand, the thermodynamic correction obtained by using the PM3 method in combination with a free energy equation for a primitive model gives a theoretical funded prediction for the phase diagram.

In Table 3, we compare the theoretical predictions for the I−N transition for $P = 1$ atm obtained by us and by Williamson[19] for uniaxial cores, and Tjipto−Margo and Evans[23] for biaxial cores. We observe that all of the theories predict that the transition temperature is very close to the actual value and that the packing fraction at the phase transition is underestimated, even when the biaxial cores are used. It has been observed[23,42] for systems formed by biaxial ellipsoids that the I−N phase transition shifts to higher densities by increasing biaxiality, so the opposite trend observed in Table 3 suggest that the biaxial-core theory overestimates the angular dependence of the attractive forces and then induce a shift of the phase transition to lower densities. Biaxiality decreases the density jump at the I−N transition and reduces the orientational order in the nematic phase, effects that are predicted correctly by the biaxial-core theory when compared to the uniaxial models. Also the entropy change at the phase transition is better described using biaxial-cores, an effect that can be explained because the density jump for the I−N phase transition is smaller for these models.

5. Conclusions

In this paper, we have shown the combined use of a perturbation theory for liquid crystals and PM3 calculations in order to predict the phase diagram of these systems. Calculating an estimated value of the molecular volume V_m by PM3 instead of the fitting method to thermodynamic properties, the theoretical prediction substantially improves its accuracy. The theory works on the basis of a primitive model for a real liquid crystal, assuming a decoupling of degrees of freedom and a long-range approximation for the calculation of the perturbation terms. Molecular features such as flexibility and polarity are neglected, but they introduce important effects on the phase diagram, as a recent computer simulation study has shown.[43] It would be desirable to incorporate the contributions to the free energy given by these properties. Furthermore, on the basis of the results given in Table 3, a cylindrical symmetrical core overestimates the orientational order in the nematic phase, and the density jump calculated is higher than the computer simulation predictions. Since the PM3 method clearly indicates that the molecular geometry is complex, we expect that the observed inaccuracies could be corrected extending the thermodynamic perturbation theory to molecules with more complex hard-core geometries. Finally, we want to remark that the combined use of a molecular-based thermodynamic perturbation theory and an accurate quantum mechanical method for obtaining molecular parameters give a more realistic and accurate representation of real substances phase behavior. It is encouraging that the use of accurate independent molecular-based methods (i.e., PM3 and thermodynamic perturbation methods) designed to describe different features of a real LC substance (i.e., molecular geometry and phase behavior, respectively) can give a consistent better description of the phase diagram, and reducing to the minimum the use of "fitting procedures".

Acknowledgment. The authors gratefully acknowledge the valuable discussions with Juvencio Robles (FQ-UGTO). This work received support from CONACyT (México), Grant No.

33523-E. EGS would like also to acknowledge support form CONCyTEG (Guanajuato), Grant Nos. 98-16-03-008, 99-16-203-001, and 00-16-203-0010.

References and Notes

(1) Allen, M. P.; Wilson, M. R. *J. Computer Aided Mol. Design* **1989**, *3*, 335.
(2) Frenkel, D.; Mulder, B. M. *Mol. Phys*. **1985**, *55*, 1171.
(3) Frenkel, D.; Lekkerkerker, H. N. W.; Stroobants, A. *Nature* **1988**, *332*, 822.
(4) McGrother; S. C.; Williamson, D. C.; Jackson, G. *J. Chem.* Phys. **1996**, *104*, 6755.
(5) Onsager, L. *Ann. N. Y. Acad. Sci.* **1949**, *51*, 627.
(6) Vroege, G. J.; Lekkerkerker, H. N. W. *Rep. Prog. Phys.* **1992**, *55*, 1241.
(7) Parsons, J. D. *Phys. Rev. A* **1979**, *19*, 1225.
(8) Lee, S. D. *J. Chem. Phys*. **1987**, *87*, 4972.
(9) Lee, S. D. *J. Chem. Phys*. **1988**, *89*, 7036.
(10) Camp, P. J.; Mason, C. P.; Allen, M. P.; Khare, A. A.; Kofke, D. A. *J. Chem. Phys.* **1996**, *105*, 2837.
(11) Carnahan, N. F.; Starling, K. E. *J. Chem. Phys*. **1969**, *51*, 635.
(12) Wertheim, M. S. *J. Math. Phys.* **1964**, *5*, 643.
(13) Maier, W.; Saupe, A. *Z. Naturf*. **1958**, *13*, 564.
(14) Alder, B. J.; Hetch, C. E. *J. Chem. Phys.* **1969**, *50*, 2032.
(15) Alben, R. *Mol. Cryst. Liq. Cryst*. **1971**, *13*, 193.
(16) Cotter, M. A. *J. Chem. Phys*. **1977**, *66*, 1098.
(17) Gelbart, W. M.; Baron, B. A. *J. Chem. Phys*. **1977**, *66*, 207.
(18) Linder, B.; Kromhout, R. A. *J. Chem. Phys*. **1995**, *102*, 6566.
(19) Williamson, D. C. *Mol. Phys*. **1998**, *95*, 319.
(20) Barker, J. A.; Henderson, D. *J. Chem. Phys*. **1967**, *47*, 2856.
(21) Ponce, L.; Renon, H. *J. Chem. Phys*. **1976**, *64*, 638.
(22) Gelbart, W. M.; Gelbart, A. *Mol. Phys.* **1977**, *33*, 1387.
(23) Tjipto-Margo, B.; Evans, G. T. *Mol. Phys*. **1991**, *74*, 85.
(24) Sambroski, A.; Evans, G. T. *Mol. Phys*. **1991**, *80*, 1257.
(25) De Miguel, E.; Allen, M. P. *Mol. Phys*. **1992**, *76*, 1275.
(26) Del Río, F.; Gil-Villegas, A. *J. Phys. Chem.* **1991**, *95*, 787.
(27) Gil-Villegas, A.; del Río, F. *Rev. Mex. Fis.* **1993**, *39*, 526.
(28) Gil-Villegas, A.; del Río, F.; Benavides, A. L. *Fluid Phase Eq.* **1996**, *119*, 97.
(29) Barker, J. A.; Henderson, D. *Rev. Mod. Phys*. **1976**, *48*, 587.
(30) Benavides, A. L.; del Río, F. *Mol. Phys.* **1989**, *68*, 983.
(31) Del Río, F.; Lira, L. *J. Chem. Phys.* **1987**, *87*, 7179.
(32) Benavides, A. L.; Alejandre, J.; del Río, F. *Mol. Phys.* **1991**, *74*, 321.
(33) Williamson, D. C.; Jackson, G. *Mol. Phys*. **1994**, *83*, 603.
(34) Levine, I. N., Ed. *Quantum Chemistry*; Prentice Hall: New York, 1991.
(35) Stewart, J. J. P. *J. Comput. Chem*. **1989**, *10*, 209.
(36) García, E.; Williamson, D. C.; Martinez-Richa, A. *Mol. Phys*. **2000**, *98*, 179.
(37) Telo da Gama, M. M. *Mol. Phys*. **1984**, *52*, 585.
(38) Telo da Gama, M. M. *Observations, Predictions and Simulations of Phase Transitions in Complexes Fluids*; Baus, M., Rull, L. F., Pyckaert, J. P., Eds.; Dordrecht: Kluwer, 1995, 243.
(39) Cotter, M. A. *Mol. Cryst. Liq. Cryst*. **1983**, *97*, 29.
(40) Baron, B. A.; Gelbart, W. M. *J. Chem. Phys*. **1977**, *67*, 5795.
(41) Chandrasekhar, S. *Liquid Crystals*, 2nd ed; Cambridge University Press: New York, 1992.
(42) Allen, M. P. *Liquid Crystal* **1990**, *8*, 499.
(43) Van Duijneveldt, J.; Gil-Villegas, A.; Jackson, G.; Allen, M. P. *J. Chem. Phys.* **2000**, *112*, 9092.